Evaluation of detection efficiency of a transition edge sensor at C-band wavelength

Optics & Laser Technology 192 (2025) 113414

Contents lists available at ScienceDirect

Optics and Laser Technology

journal homepage: www.elsevier.com/locate/jolt

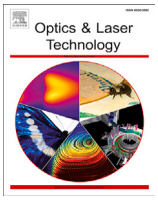

Full length article

Evaluation of detection efficiency of a transition edge sensor at C-band wavelength

Takeshi Jodoi[a, b,*], Tetsuya Tsuruta[a], Mauro Rajteri[c], Daiji Fukuda[a]

[a] National Institute of Advanced Industrial Science and Technology, 1-1-1, Umezono, Tsukuba, 305-8563, Ibaraki, Japan
[b] The University of Tokyo, 2-11-16, Yayoi, Bunkyo, 113-8656, Tokyo, Japan
[c] Istituto Nazionale di Ricerca Metrologica, Strada delle Cacce 91, 10135, Torino, Italy

HIGHLIGHTS

- We developed a calibration system for the C-band wavelength using laser pulses.
- Initial states were generated via laser by switching acoustic optical module.
- Input state photon statistics were evaluated by a second-order correlation function.
- Wavelength-dependent detection efficiency was precisely determined.
- Detection efficiency was evaluated by comparing experimental and simulation values.

ARTICLE INFO

Keywords:
Transition edge sensor
System detection efficiency
Wavelength-dependent
Continuous wave

ABSTRACT

Photon-number-resolving detectors face strict demands regarding detection efficiency to meet the needs of quantum information processing. We constructed a system that can accurately evaluate system detection efficiency of a photon-number-resolving detector. We generated an optical pulse containing an arbitrary number of photons for the initial states by attenuated laser light; this pulse was used to evaluate the detection efficiency of the device under test. To generate this pulse, we modulated a continuous wavelength tunable laser using an acoustic optical modulator. From the photon statistics of the initial states, we found a second-order correlation function that was almost 1 at any wavelength, and these photon statistics followed a Poisson distribution. For the device under test, we evaluated the detection efficiency of a transition edge sensor and we employed two methods to calculate the number of detected photons. This value was calculated based on each photon state (method 1) or based on the zero photon state by assuming a Poisson distribution (method 2). Although the results of both methods were comparable within the range of uncertainty, method 2 yielded smaller uncertainty than method 1. We found that the wavelength-dependent detection efficiency was explained by the photon absorptance characteristics of the device under test. Additionally, the system detection efficiency varied from approximately 87 % to 93 %, and the expanded uncertainty values of methods 1 and 2 were 4.1 % and 1.5 %, respectively. This system enables the accurate evaluation of quantum states of photons at various wavelengths.

1. Introduction

The quantum light source and the photon-number-resolving detector (PNRD) are essential elements for the quantum information processing [1–4] and quantum communication [5–7]. Quantum light sources such as single-photon sources and squeezed light sources are utilized to generate non-classical states of photons, but necessitate high performance. For example, a second-order correlation function of a single-photon source must be nearly zero, and the squeezing level of a squeezed light source must be at least 12.8 dB to realize quantum error correction [8]. When evaluating these quantum light sources, the photon detection technology is also important. For example, PNRDs such as transition edge sensors (TESs) are also utilized to distinguish the number of photons accurately [9,10]. Therefore, TESs are expected to be valuable in the fields of quantum optics, and are already used in optical quantum computers to detect photons from the squeezed light source [4,11]. In studies in this field,

* Corresponding author at: National Institute of Advanced Industrial Science and Technology, 1-1-1, Umezono, Tsukuba, 305-8563, Ibaraki, Japan.
Email address: t.joudoi@aist.go.jp (T. Jodoi).

https://doi.org/10.1016/j.optlastec.2025.113414
Received 9 February 2025; Received in revised form 21 May 2025; Accepted 18 June 2025
Available online 25 July 2025

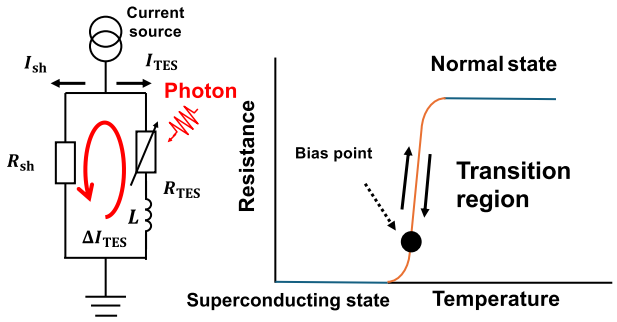

Fig. 1. The principle of operation of a TES: The TES is voltage-biased in superconducting-normal transition region through electrothermal feedback. R_{sh}, shunt resistance; I_{sh}, current flowing through shunt resistance; L, kinetic inductance; R_{TES}, the resistance of TES at bias point; I_{TES}, current flowing through TES; When a photon is absorbed by the TES, it increases the resistance of the TES and generates a current change ΔI_{TES}. This current change generates signals from which we obtain the photon number distribution.

the accurate evaluation of photons from a quantum source requires high performance photon detectors. Broadband light sources have also attracted attention for the generation of quantum entangled pairs, which are an essential part of quantum information processing [12,13]. For these reasons, PNRDs, such as TESs, must also have broadband high detection efficiency according to the wavelength of the photon sources. Therefore, accurate investigations of the wavelength-dependent detection efficiency of TES devices at telecommunication wavelengths are increasingly important. A TES is a highly sensitive microcalorimeter used to detect photons directly through steep resistance changes in the transition area (Fig. 1). The TES is voltage-biased at the superconducting transition, and when a photon is absorbed by the TES, the temperature of the TES increases according to the photon's energy. This temperature increase causes a rise in resistance, which is detected through the change in current across the TES. TESs have promising performance, exhibiting up to 100 % quantum efficiency, sensitivity to broadband wavelengths, and accurate distinguishment of photons. For these reasons, TESs are expected to be used for many applications, such as bioimaging [14,15], quantum information processing and communication, optical sensing, and astronomy [16,17]. In principle, a TES can measure the number of photons in a monochromatic light pulse and distinguish various photon number distributions from these measurement results. To accurately evaluate the photon number states in pulses, it is necessary to develop a measurement system with high system detection efficiency (SDE). SDE is defined by the probability of indicating a detection event of one photon incident upon the detector's input plane [18]. In the case of PNRDs such as TESs, it is necessary to obtain an accurate average number of detected photons based on the response from the photon number distribution of the TES and the number of input photons at relevant wavelengths in order to calculate detection efficiency accurately. Furthermore, a high SDE is also important for quantum information processing. A PNRD must have an SDE of almost 100 %, a 0 % dark count rate, and photon-number-resolving ability at communication wavelengths. A TES in which an optical cavity is embedded for high photon absorption is one of the promising PNRDs to meet these strict requirements. However, the photon absorption performance of the cavity should still be well characterized for the application. To date, high photon absorption efficiency in TESs with detection efficiency exceeding 95 %, has already been achieved using an optical cavity [19–21]. To achieve higher SDE by TES with optical cavity, it is necessary to improve the measurement system at C-band. In this paper, we report the dependence of the system detection efficiency on the wavelength using pulsed light generated from continuous-wave laser in the C-band. To investigate the wavelength-dependent detection efficiency, we developed a calibration system with a wavelength-tunable pulsed laser source, composed of an external cavity diode laser (ECDL) and acoustic optical module (AOM). We generated an optical pulse with an arbitrary average number of photons as the initial input state, and fed this signal into the device under test (DUT), which was a PNRD coupled via an optical fiber. We identified the system detection efficiency based on the photon number distribution from the response of the DUT and initial input state. Additionally, we evaluated the photon number distribution obtained from the DUT and the stability of laser power to ensure the validity of the generated initial input state. To clarify the initial input state, we evaluated this calibration system with $g^{(2)}$, a Poisson distribution, and Allan variance. Furthermore, we calculated the detection efficiency for each wavelength and evaluated the wavelength dependence, comparing it to simulation results. We show the experimental setup and the detection efficiency results in the C-band. The rest of this paper is structured as follows. Section 2 describes our experimental methods, while Section 3 presents the results. Section 4 discusses these findings. Finally, Section 5 summarizes the paper and provides concluding remarks.

2. Experimental methods

In this experiment, we used superconducting bilayer films of titanium and gold in the TES, embedded in an optical cavity designed for use in the C-band. The design and performance of this TES are summarized in Table 1. The TES has a reasonable energy resolution of 0.38 eV. Supplementary Appendix A shows the influence of energy resolution on the uncertainties of this measurement system. From this appendix, we found that this energy resolution is enough to resolve photon numbers for C-band wavelength photons corresponding to 0.8 eV/photon. In addition to this, we employed UHNA7 optical fiber to improve the alignment between the sensitive area of TES and optical fiber. The 12 μm square size effectively matches the mode field diameter of the optical fiber coupled to the TES. Fig. 2(a) shows the experimental measurement setup used in this study. To generate laser pulses including some number of photons as an input photon state for the DUT, we first apply a continuous wavelength (CW) laser source. In this study, the CW laser source was a tunable wavelength laser based on an ECDL, which covers the wavelength range from 1510 nm to 1570 nm. The spectrum width of the ECDL source is typically 0.1 nm. However, its spectrum also includes an amplified spectrum emission (ASE), which ranges from 1470 nm to over 1600 nm; this would affect the accuracy of the power measurement performed by a reference detector. Therefore, to remove the ASE, we used a tunable bandpass filter (BPF) with a transmission bandwidth of 1 nm by adjusting its center wavelength to the emission line of the ECDL. After passing through the BPF, the laser light is divided into two paths using a fiber coupler, and the spectrum of one branch is monitored by a spectrum analyzer. Fig. 2(b) shows the spectra with and without BPF, showing the successful removal of the ASE with an extinction ratio of 19.9 dB. Next, we used an AOM to chop the CW laser to generate laser pulses. Fig. 2(c) shows the results of time-dependent pulse shape measurement using a high speed photodiode, showing that the full width at half maximum (FWHM) of the pulse was 11.3 ns. The extinction ratio of the AOM was measured as −32 dB, which was within the uncertainty of the power measurement. Supplementary Appendix B shows the influence of the extinction ratio on this measurement system with changing the repetition frequencies and wavelengths. In this

Table 1
The design and performance of this TES.

Design	TES size	12 μm × 12 μm
	Material	Ti 22 nm/Au 15 nm
Performance	Transition temperature	0.340 K
	Time constant	597 ns
	Energy resolution	0.38 eV

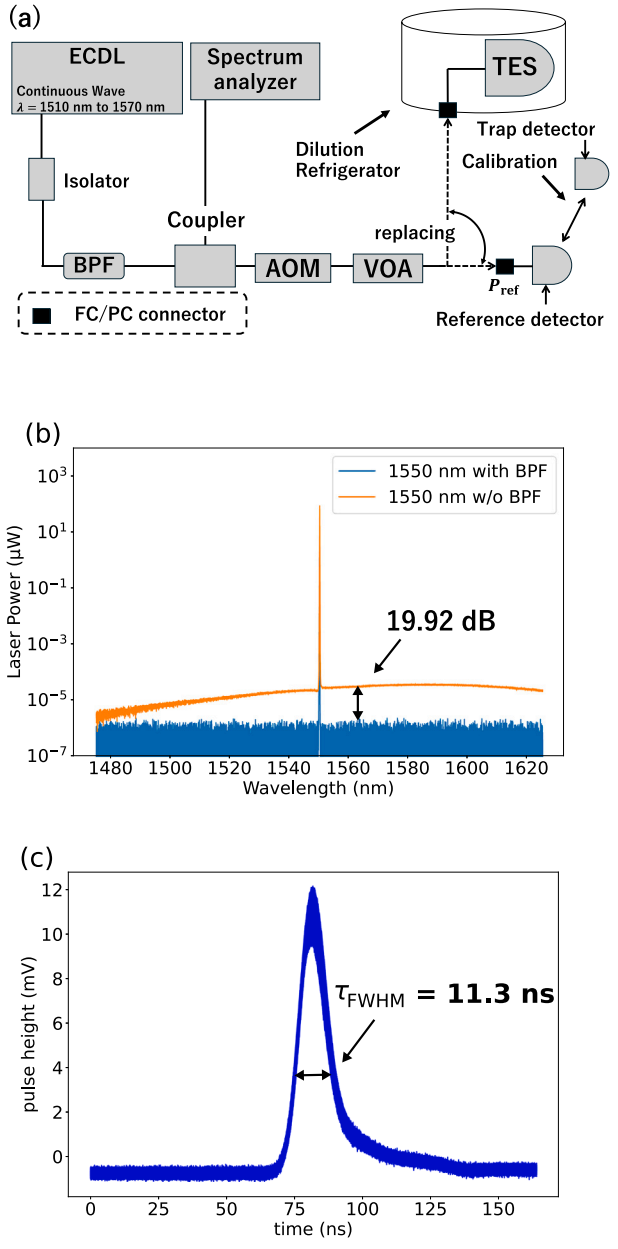

Fig. 2. (a) The setup of our measurement system. We pulsed a continuous wave from the ECDL and BPF via AOM switching. ECDL, external cavity diode laser; BPF, band pass filter; AOM, acoustic optical module; VOA, variable optical attenuator; TES, transition edge sensor. (b) Outputs from the ECDL at 1550 nm. The BPF reduced noise approximately 19.9 dB over 1560 nm. (c) The pulse being converted by the AOM. The τ_{FWHM} of this pulse is 11.3 ns.

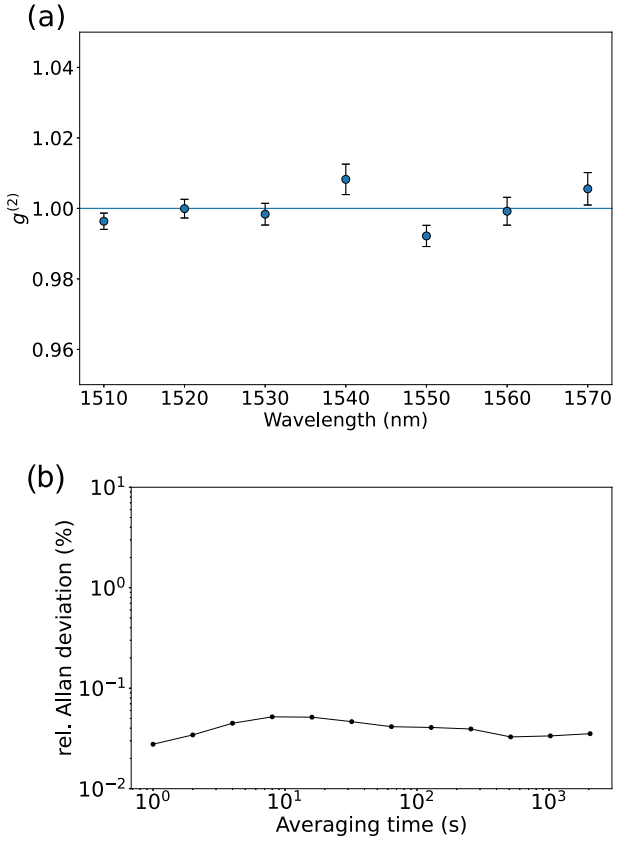

Fig. 3. (a) The relationship between $g^{(2)}$ and the wavelength. $g^{(2)}$ is nearly 1 at any wavelength, and it was confirmed that the pulse in our measurement system follows a Poisson distribution. The standard uncertainties were deduced from the uncertainties of $P(n)$ at each photon state. (b) The relative Allan deviation with averaging time. This value is 0.05 % at most, which is not significant relative to the total uncertainty of the detection efficiency measurement.

experiment, the repetition frequency is all set to 100 kHz for any wavelengths. Therefore, we found that the extinction ratio is negligibly small compared to the uncertainty of the power measurement in the reference detector. Finally, the laser pulses were sent to a power meter via a variable optical attenuator (VOA). The power meter was calibrated to our national standard, and the measured power is a very important parameter for the extraction of the input photon number. After the power measurement, we heavily attenuated the laser pulses using the VOA to set a certain average number of photons. Then, we switched the optical fiber to send the prepared input photon states to the DUT using the same optical fiber. We recorded observed signal pulses from the DUT and obtained their photon number distributions. The photon number distribution is fitted with the sets of Gaussian functions to derive the detection probabilities for each photon state, which results in the detected average photon number. Finally, we calculated the detection efficiency by dividing the detected average photon number by input average photon number.

It is worth considering what kind of photon statistics could be expected with these heavily attenuated and AOM-chopped laser pulses for a specific DUT, such as a TES. To clarify this point, we evaluated an autocorrelation function by measuring $g^{(2)}$ values using the TES. In the photon number states, $g^{(2)}$ can be described as $g^{(2)} = n^{(2)}/\langle n_{exp}\rangle^2$, where $n^{(2)} = \sum_{n=2}^{\infty} \frac{n!}{(n-2)!} P(n)$, $\langle n_{exp}\rangle = \sum_{n=0}^{\infty} nP(n)$, and $P(n)$ is the probability of photon state n in a certain photon distribution. To evaluate the dependence of $g^{(2)}$ values on the wavelength, we measured the photon number distributions with the TES as an average incident photon number of 3 photons/pulse in different wavelength ranges from 1510 nm to 1570 nm in steps of 10 nm. Fig. 3(a) shows the obtained $g^{(2)}$ dependence on the wavelengths with error bar. As shown, $g^{(2)}$ is close to 1 in all wavelength regions, which indicates that the photon statistics of the prepared input state obey a Poisson distribution. Additionally, we evaluated the stability of the laser power of the prepared input photon state. We measured the average laser power at intervals of 1 s and deduced a relative Allan deviation, which is a ratio between the Allan deviation and the average measured power, as shown in Fig. 3(b) [22,23]. The relative Allan deviation is below 0.05 % in the integration time up to 10^3 s, which is not significant relative to the total uncertainty of the detection efficiency measurement. Still, we ensured that all measurements, such as determination of laser power, switching of the optical fiber, and the DUT

measurement were finished within five minutes to minimize laser power drift during these procedures.

The average number of input photons is expressed by

$$\mu'_{\text{in}} = P_{\text{ref}} \times 10^{-\frac{A}{10}} \times \frac{1}{f} \times \frac{\lambda}{hc} \tag{1}$$

where P_{ref} is the value of the reference detector, A is the value of the attenuator expressed in dB, f is the repetition frequency of the laser pulses, h is the Planck constant, c is the speed of light, and λ is the wavelength of an input photon. However, in this experiment, it is necessary to consider a power difference due to reflection on the fiber end face in the measurement of P_{ref}. When measuring the power using a reference detector, the laser light enters the air from the optical fiber before reaching the power meter; thus, optical reflection occurs at the fiber end owing to the refractive index difference. In contrast, when we introduce photons to the TES, we connect fiber to fiber, and no reflection occurs at the fiber end faces. For that reason, we need to clarify the extent to which the laser power is reflected at the end face. We should consider the effect of the reflection R_{ref} to determine the correct average number of photons in the prepared input photon state; thus, Eq. (1) can be modified to obtain the following equation:

$$\mu_{\text{in}} = P_{\text{ref}} \times 10^{-\frac{A}{10}} \times \frac{1}{f} \times \frac{\lambda}{hc} \times \frac{1}{1-\text{R}_{\text{ref}}} \tag{2}$$

This R_{ref} can be evaluated by using a circulator, fiber-optic retroreflector, and optical absorber, and we determined the R_{ref} in this calibration system was 3.86 %. In the following detection efficiency determination experiments, we used the Ti/Au optical TES with a 12 μm × 12 μm sensitive area, as described in Table 1. We irradiated the TES $N = 10^4$ times to construct the photon number distributions observed in the TES. From the photon number distributions, we deduced an average photon number μ_{det}, and finally, we determined the detection efficiency of the DUT η as

$$\eta = \mu_{\text{det}}/\mu_{\text{in}} \tag{3}$$

3. Results and calculation methods

As discussed in Section 2, we calculated the average number of photons detected by the TES using the prepared input photon state. Fig. 4(a) shows the typical response signals of the TES upon irradiating the input state at the wavelength of 1550 nm. The pulse heights of the signals are discretized; these heights correspond to the detection events with the photon number n. Fig. 4(b) shows the histogram of a photon number distribution constructed by extracting the pulse height from each response signal. From this distribution, we can deduce the detection probability $P(n)$ of the photon number of state n as

$$P(n) = S(n)/N \tag{4}$$

where $S(n)$ denotes the counts of the n-th peak event, and N denotes the counts of total events (for our case, $N = 10^4$).

Using Eq. (4), we can easily derive the average photon number in the observed photon number distribution as

$$\mu_{\text{det}} = \sum_{n=0}^{n_{\max}} nP(n) \tag{5}$$

However, Eq. (5) requires additional consideration because it is necessary to determine which photon numbers of $n_{\max}$ should be considered. To solve this problem, we have employed two methods and compared the results.

3.1. Method 1: maximum photon number truncation method

First, we define the maximum photon number state $n_{\max}$ and truncate the events of $n \geq n_{\max}$. As discussed in Section 2, the photon number

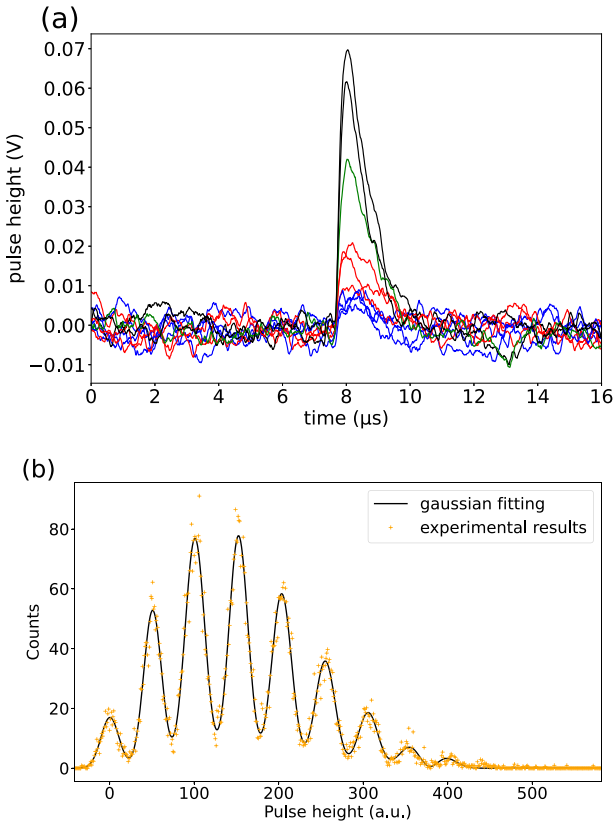

Fig. 4. (a) This figure shows the signals obtained from the TES, when triggered by light pulse. These signals indicate that the TES can accurately distinguish each photon. (b) This graph shows the histogram of the pulse amplitudes with multi-Gaussian fitting. We used the fitting function on the photon number distribution to obtain the possibility and standard deviation of each photon state. We defined the maximum photon states according to a Poisson distribution.

distribution of the prepared input state follows a Poisson distribution. Therefore, it is a good approximation to assume that the photon number distribution measured by the TES also obeys a Poisson distribution. The Poisson distribution is expressed by $P_{\text{poisson}}(n|\mu) = (\eta\mu)^n \exp(-\eta\mu)/n!$, where η is the expected detection efficiency, μ is the mean photon number of the TES, and n is the number of photon states. From this equation, we adopt the maximum number of photon states $n_{\max}$, which satisfies

$$\sum_{n=0}^{n_{\max}} nP_{\text{poisson}}(n|\mu) \geq 0.995 \tag{6}$$

We adopted $n_{\max} = 9$ as a typical value at the incident photon number of 3 photons/pulse. In order to calculate the P_n on Eq. (5), we fitted the photon number distribution using the formula of the sum of Gaussian fitting. The fitting function is as follows:

$$f(x) = \sum_{n=0}^{n_{\max}} \frac{S(n)}{\sqrt{2\pi}\sigma_n} \exp\left(-\frac{(x-b_n)^2}{2\sigma_n^2}\right) \tag{7}$$

where b is the median and σ is the standard deviation. In Fig. 4(b), the result fitted using Eq. (7) is also shown as a black solid line. From this Gaussian function, the number of photons at each photon state is expressed by $S(n) = \sqrt{2\pi}\text{A}_n\sigma_n$, where A_n is the amplitude of the Gaussian distribution and σ_n is the standard deviation at n photon states. Additionally, we calculated the standard error as $\Delta S(n) = \sqrt{2\pi((\delta\text{A}_n\sigma_n)^2 + (\text{A}_n\delta\sigma_n)^2)}$, where $\Delta S(n)$ is the standard error

Table 2
The average number of detected photons with uncertainty from each method. The unit of μ_{det} is photon/pulse.

Wavelength (nm)	μ_{det} with $\Delta\mu_{det}$ on Eq. (5) (photon/pulse)	μ_{det} with $\Delta\mu_{det}$ on Eq. (9) (photon/pulse)
1510	2.68 ± 0.05	2.68 ± 0.02
1520	2.76 ± 0.06	2.77 ± 0.02
1530	2.89 ± 0.04	2.85 ± 0.02
1540	2.97 ± 0.05	2.97 ± 0.02
1550	3.03 ± 0.04	3.05 ± 0.02
1560	3.10 ± 0.04	3.10 ± 0.02
1570	3.05 ± 0.07	3.08 ± 0.02

at n photon states. The uncertainty of each photon state is expressed by $\Delta P(n) = \Delta S(n)/N$. From these equations, we calculate the uncertainty of this method using the root sum squared:

$$\Delta\mu_{\mathrm{det}}{}^2 = \sum_{n=0}^{n_{\max}} (n\times\Delta P(n))^2 + \left((n_{\max}+1)\times\left(1-\sum_{n=0}^{n_{\max}} P(n)\right)\right)^2 \quad (8)$$

We deduce the μ_{det} and uncertainty of this method $\Delta\mu_{det}$ from Eqs. (5) and (8), and Table 2 shows the average number of detected photons at each wavelength.

3.2. Method 2: zero photon probability method

In the second method, we calculate the observed average photon number from the zero photon state. As discussed in Section 3.1, it is a good approximation to assume that the photon number distribution of the TES follows a Poisson distribution. Therefore, we can directly calculate it from the following equation:

$$\mu_{\mathrm{det}} = -\log P(0) \quad (9)$$

where $P(0)$ is the detected probability of the zero photon state. We can also calculate the uncertainty of method 2 through the use of uncertainty at the zero photon state:

$$\Delta\mu_{\mathrm{det}} = \Delta P(0)/P(0) \quad (10)$$

From Eqs. (9) and (10), we can also calculate the detected photons and uncertainty of this method at each wavelength, with the results shown in Table 2. From these results, we found that both methods yield the same value regarding the number of detected photons. However, the uncertainty $\Delta\mu_{det}$ differs between methods. In method 1, we truncate the photon number states according to the maximum photon number state, and there is uncertainty at each photon state according to Eq. (7).

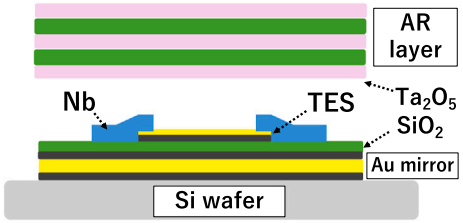

Fig. 5. Cross-sectional view of this TES with optical cavity.

In contrast, method 2 does not involve truncation, and we do not need to consider uncertainty other than that at the zero photon state. Therefore, the uncertainty of method 2 is smaller than that of method 1.

4. Discussion

In this section, we discuss how the detection efficiencies η obtained by the two methods can be validated and matched to the expected values. The TES used in the detection efficiency calibration was designed to have high photon absorption efficiency through the use of an optical cavity, which consisted of stacked layers of dielectric films of Ta_2O_5 and SiO_2 and a gold reflection mirror, as shown in Fig. 5. The optical absorption performance can be calculated based on the refractive indices and thicknesses of these films [20].

To evaluate this calibration system, the uncertainty of each component in the system must be calculated. Thus, we evaluated the uncertainty of the reference detector and optical attenuator. We calibrated the reference detector by using a trap detector following national standards. Thus, we also investigated the calibration uncertainty and linearity of the trap detector, as well as the calibration uncertainty of the reference detector. Additionally, the laser stability must be considered as a component of the uncertainty. As described in Section 3, we obtained the laser stability using the Allan variance. The maximum value of the Allan variance was 0.05 %, and we used this maximum value as the uncertainty of this laser. When introducing photons to the TES, we attenuated the power using the VOA. We must also consider the uncertainty of this attenuation value. From these experimental data, we found that the maximum uncertainty of this attenuator was 0.24 %. Finally, we combined these uncertainty values with the uncertainty $\Delta\mu_{det}/\mu_{in}$ from methods 1 and 2. Table 3 presents the uncertainty budget of this calibration system. The combined uncertainty is expressed by the square root of the sum of the squares of each uncertainty [24]. The results show that the maximum uncertainty of method 1 is 2.1 % and that of method 2 is 0.77 %. From these results, we calculated the SDE at each wavelength using Eq. (3). Table 4 shows the SDE and combined uncertainty at each

Table 3
Uncertainty budget.

Uncertainty components		Value	Divider	Type	Distribution	Rel. standard uncertainty
P_{ref}	Calibration of trap detector	0.22 %	2	B	Normal	0.11 %
	Linearity of trap detector	0.14 %	$2\sqrt{3}$	B	Rectangle	0.04 %
	Calibration of reference detector	0.09 %	1	A	Normal	0.04 %
	Laser stability	0.05 %	1	A	Normal	0.05 %
Optical attenuation	Attenuation	0.010 dB	1	A	Normal	0.24 %
μ_{det}	Method 1	2.0 %	1	A	Normal	2.0 %
	Method 2	0.72 %	1	A	Normal	0.72 %
Combined standard uncertainty					Method 1	2.1 %
					Method 2	0.77 %
Expanded uncertainty (k = 2, 95 % confidence)					Method 1	4.1 %
					Method 2	1.5 %

Table 4
The SDE and uncertainty of SDE at each wavelength.

Wavelength (nm)	η_{SDE} with $\Delta\eta_{SDE}$ on Eq. (5) (%)	η_{SDE} with $\Delta\eta_{SDE}$ on Eq. (9) (%)
1510	88.3 ± 1.6	88.40 ± 0.60
1520	87.0 ± 1.8	87.48 ± 0.68
1530	91.0 ± 1.3	89.80 ± 0.66
1540	89.0 ± 1.5	88.84 ± 0.68
1550	91.4 ± 1.3	90.83 ± 0.75
1560	91.7 ± 1.3	91.89 ± 0.77
1570	92.4 ± 2.0	93.02 ± 0.77

wavelength. Fig. 6(a) and (b) show some comparisons between η values with method 1 or 2, respectively, and the simulation results. We also added the combined uncertainty from both methods to these figures. For both methods, the wavelength dependencies of the calibrated η agreed well with the expected values. The wavelength trend of η in method 2 changes more smoothly compared to that of method 1, which might be due to the effect of the maximum photon number truncation in method 1. In previous research, they evaluated the wavelength-dependent optical structure by measuring reflectance of the optical cavity [25]. In this research, we pulsed continuous wave by switching AOM and compared the result to simulated photon absorptance curve. This is the first report about photon-based detection efficiency at C-band with pulsing continuous wave. From Fig. 6, we found the values of the calibrated η are a few percent lower than the expected values. The reason for this difference is considered to be a loss in the fiber splicing coupled to the TES or in the fiber alignment [21]. We plan to clarify these losses in future work.

5. Summary and conclusions

In this experiment, we evaluated the dependency of SDE on wavelength in the C-band. To exploit the high photon-number-resolving ability of a TES, we succeeded in pulsing a continuous-wave laser through AOM switching and detecting photons at an arbitrary wavelength in the C-band. We also confirmed that the pulse in our setup followed a Poisson distribution from the view of $g^{(2)}$. Additionally, we evaluated the power stability of AOM-chopped laser pulses using Allan variance and found that the laser pulse had sufficient stability to evaluate the SDE of this calibration system. We employed two methods to evaluate the SDE and found that both were consistent with the photon absorptance of the TES. The expanded uncertainty of method 2 was 1.5 %, which is smaller than that of method 1 because of the truncation and total number of errors at each photon state. As a result, we succeeded in evaluating the SDE of PNRD in a wide wavelength range with an uncertainty of 1.5 %, as well as constructing a calibration system with a CW tunable laser and an AOM. These results provide a major contribution to quantum technology because this calibration system enables the accurate evaluation of quantum states of photons at a wide range of wavelengths. Furthermore, this precise evaluation of wavelength dependence will provide useful information to evaluate the characteristics of optical cavities, thus promoting the development of PNRDs with near 100 % detection efficiency.

CRediT authorship contribution statement

Takeshi Jodoi: Writing – original draft, Visualization, Methodology, Investigation, Formal analysis, Data curation, Conceptualization. **Tetsuya Tsuruta:** Writing – review & editing, Supervision, Methodology, Investigation, Conceptualization. **Mauro Rajteri:** Writing – review & editing, Supervision, Methodology, Conceptualization. **Daiji Fukuda:** Writing – review & editing, Supervision, Methodology, Investigation, Formal analysis, Data curation, Conceptualization.

Declaration of competing interest

The authors declare that they have no known competing financial interests or personal relationships that could have appeared to influence the work reported in this paper.

Acknowledgments

This work was supported in part by JST Moonshot R&D Program Grant Number JPMJMS2064-6, International Exchange Program of National Institute of Information and Communication (NICT), Program for bridging the gap between R&D and the ideal society and generating economic and social value (BRIDGE), Cross-ministerial Strategic

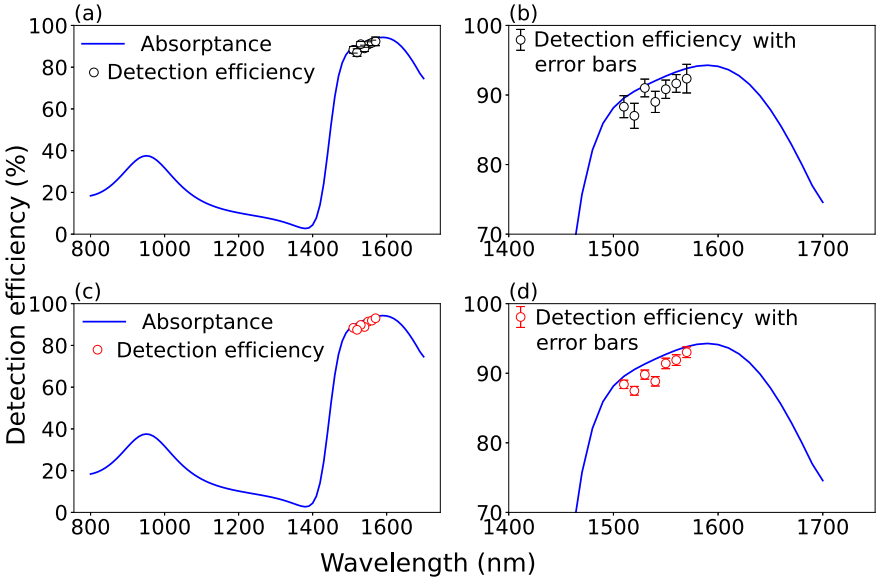

Fig. 6. (a) Comparison between measured system detection efficiency from method 1 and the simulated photon absorptance of this TES. (b) Enlarged figure of measured system detection efficiency with error bar from method 1 and the simulated photon absorptance from 1400 nm to 1750 nm wavelength. (c) Comparison between measured system detection efficiency from method 2 and the simulated photon absorptance of this TES. (d) Enlarged figure of measured system detection efficiency with error bar from method 2 and the simulated photon absorptance from 1400 nm to 1750 nm wavelength.

Innovation Promotion Program (SIP), and JSPS KAKENHI Grant Number 24K01374.

Appendix A. Supplementary data

Supplementary data to this article can be found online at doi:10.1016/j.optlastec.2025.113414.

Data availability

Data will be made available on request.

References

[1] M. Endo, R. He, T. Sonoyama, K. Takahashi, T. Kashiwazaki, T. Umeki, S. Takasu, K. Hattori, D. Fukuda, K. Fukui, et al., Non-Gaussian quantum state generation by multi-photon subtraction at the telecommunication wavelength, Opt. Express 31 (8) (2023) 12865–12879.
[2] S. Konno, W. Asavanant, F. Hanamura, H. Nagayoshi, K. Fukui, A. Sakaguchi, R. Ide, F. China, M. Yabuno, S. Miki, et al., Logical states for fault-tolerant quantum computation with propagating light, Science 383 (6680) (2024) 289–293.
[3] E. Knill, R. Laflamme, G.J. Milburn, A scheme for efficient quantum computation with linear optics, Nature 409 (6816) (2001) 46–52.
[4] L.S. Madsen, F. Laudenbach, M.F. Askarani, F. Rortais, T. Vincent, J.F. Bulmer, F.M. Miatto, L. Neuhaus, L.G. Helt, M.J. Collins, et al., Quantum computational advantage with a programmable photonic processor, Nature 606 (7912) (2022) 75–81.
[5] P.A. Hiskett, D. Rosenberg, C.G. Peterson, R.J. Hughes, S. Nam, A. Lita, A. Miller, J. Nordholt, Long-distance quantum key distribution in optical fibre, New J. Phys. 8 (9) (2006) 193.
[6] Y. Adachi, T. Yamamoto, M. Koashi, N. Imoto, Simple and efficient quantum key distribution with parametric down-conversion, Phys. Rev. Lett. 99 (18) (2007) 180503.
[7] D.H. Smith, G. Gillett, M.P. De Almeida, C. Branciard, A. Fedrizzi, T.J. Weinhold, A. Lita, B. Calkins, T. Gerrits, H.M. Wiseman, et al., Conclusive quantum steering with superconducting transition-edge sensors, Nat. Commun. 3 (1) (2012) 625.
[8] N.C. Menicucci, Fault-tolerant measurement-based quantum computing with continuous-variable cluster states, Phys. Rev. Lett. 112 (12) (2014) 120504.
[9] K. Irwin, An application of electrothermal feedback for high resolution cryogenic particle detection, Appl. Phys. Lett. 66 (15) (1995) 1998–2000.
[10] K.D. Irwin, G.C. Hilton, Transition-edge sensors, Cryog. Part. Detect. (2005) 63–150.
[11] K. Wakui, Y. Eto, H. Benichi, S. Izumi, T. Yanagida, K. Ema, T. Numata, D. Fukuda, M. Takeoka, M. Sasaki, Ultrabroadband direct detection of nonclassical photon statistics at telecom wavelength, Sci. Rep. 4 (1) (2014) 4535.
[12] G. Brida, V. Caricato, M. Fedorov, M. Genovese, M. Gramegna, S. Kulik, Characterization of spectral entanglement of spontaneous parametric-down conversion biphotons in femtosecond pulsed regime, Europhys. Lett. 87 (6) (2009) 64003.
[13] M. Okano, R. Okamoto, A. Tanaka, S. Subashchandran, S. Takeuchi, Generation of broadband spontaneous parametric fluorescence using multiple bulk nonlinear crystals, Opt. Express 20 (13) (2012) 13977–13987.
[14] D. Fukuda, K. Niwa, K. Hattori, S. Inoue, R. Kobayashi, T. Numata, Confocal microscopy imaging with an optical transition edge sensor, J. Low Temp. Phys. 193 (5–6) (2018) 1228–1235.
[15] K. Niwa, T. Numata, K. Hattori, D. Fukuda, Few-photon color imaging using energy-dispersive superconducting transition-edge sensor spectrometry, Sci. Rep. 7 (1) (2017) 45660.
[16] W.B. Doriese, K.M. Morgan, D.A. Bennett, E.V. Denison, C.P. Fitzgerald, J.W. Fowler, J.D. Gard, J.P. Hays-Wehle, G.C. Hilton, K.D. Irwin, et al., Developments in time-division multiplexing of X-ray transition-edge sensors, J. Low Temp. Phys. 184 (1–2) (2016) 389–395.
[17] S.J. Smith, J.S. Adams, S.R. Bandler, S. Beaumont, J.A. Chervenak, E.V. Denison, W.B. Doriese, M. Durkin, F.M. Finkbeiner, J.W. Fowler, et al., Performance of a broad-band, high-resolution, transition-edge sensor spectrometer for X-ray astrophysics, IEEE Trans. Appl. Supercond. 31 (5) (2021) 1–6.
[18] J.C. Bienfang, J. Bienfang, T. Gerrits, P. Kuo, A. Migdall, S. Polyakov, O.T. Slattery, Single-Photon Sources and Detectors Dictionary, US Department of Commerce, National Institute of Standards and Technology, 2023.
[19] A.E. Lita, A.J. Miller, S.W. Nam, Counting near-infrared single-photons with 95% efficiency, Opt. Express 16 (5) (2008) 3032–3040.
[20] D. Fukuda, G. Fujii, T. Numata, K. Amemiya, A. Yoshizawa, H. Tsuchida, H. Fujino, H. Ishii, T. Itatani, S. Inoue, et al., Titanium-based transition-edge photon number resolving detector with 98% detection efficiency with index-matched small-gap fiber coupling, Opt. Express 19 (2) (2011) 870–875.
[21] R. Kobayashi, K. Hattori, S. Inoue, D. Fukuda, Development of a fast response titanium-gold bilayer optical TES with an optical fiber self-alignment structure, IEEE Trans. Appl. Supercond. 29 (5) (2019) 1–5.
[22] T. Gerrits, A. Migdall, J.C. Bienfang, J. Lehman, S.W. Nam, J. Splett, I. Vayshenker, J. Wang, Calibration of free-space and fiber-coupled single-photon detectors, Metrologia 57 (1) (2020) 015002.
[23] D.W. Allan, Statistics of atomic frequency standards, Proc. IEEE 54 (2) (1966) 221–230.
[24] I. Iso., B. Oiml, Guide to the Expression of Uncertainty in Measurement, Aenor, 1993.
[25] A.E. Lita, B. Calkins, L. Pellouchoud, A.J. Miller, S. Nam, Superconducting transition-edge sensors optimized for high-efficiency photon-number resolving detectors, in: Advanced Photon Counting Techniques IV, vol. 7681, SPIE, 2010, pp. 71–80.